THE ASTROPHYSICAL JOURNAL, 553:L109–L113, 2001 June 1

OVERVIEW OF THE *ROSAT* NORTH ECLIPTIC POLE SURVEY

J. P. HENRY,[1] I. M. GIOIA,[1,2] AND C. R. MULLIS[1]
Institute for Astronomy, University of Hawai'i, 2680 Woodlawn Drive, Honolulu, HI 96822
W. VOGES, U. G. BRIEL, AND H. BÖHRINGER
Max-Planck-Institut für extraterrestrische Physik, Giessenbachstrasse Postfach 1603, D-85741 Garching, Germany
AND
J. P. HUCHRA
Harvard-Smithsonian Center for Astrophysics, 60 Garden Street, Cambridge, MA 02138
Received 2000 October 2; accepted 2001 April 21; published 2001 May 21

ABSTRACT

We have used the *ROSAT* All-Sky Survey (RASS) observations at the north ecliptic pole (NEP) to construct a catalog of X-ray–emitting objects that is both deep and contiguous. We give here an overview of this NEP Survey. Our catalog fully exploits the capabilities of the RASS since the only criterion for inclusion is the source significance and location on the sky. There are 445 unique sources above a flux of $\sim 2 \times 10^{-14}$ ergs s^{-1} cm^{-2} (0.5–2.0 keV) in the 80.7 deg^2 region that we consider. We have optically identified 99.6% of these sources and have obtained redshifts for the extragalactic objects. The main constituents of the catalog are active galactic nuclei (AGNs; 49.0%), stars (34.3%), and groups and clusters of galaxies (14.4%). We provide the NEP Survey selection function (solid angle searched above a given flux limit), the AGNs, the clusters of galaxies, and the BL Lacertae X-ray log $N(>S)$–log S distribution as well as the catalog redshift distributions for AGNs and clusters.

Subject headings: catalogs — surveys — X-rays: general

1. INTRODUCTION

Determining the statistical properties of all objects found in a contiguous region of the sky in a certain wavelength band is one of the most fundamental investigations in observational astronomy. During the 1970s, a number of catalogs of X-ray–emitting objects over nearly the entire sky were constructed (Cooke et al. 1978; Forman et al. 1978; Piccinotti et al. 1982; Wood et al. 1984). These catalogs were relatively shallow because nonimaging instrumentation was used to construct them.

Imaging experiments provide a considerable improvement in sensitivity, usually at the expense of relatively narrow fields of view. Most imaging observations in X-ray astronomy are of preselected targets since it is very time-consuming to construct an unbiased survey of adequate solid angle with this type of instrumentation. However, it is possible to construct a nearly unbiased survey by considering those objects found serendipitously in each field after excluding a small region containing the target. The advantage of this approach is that the entire data set from the mission is available, yielding hundreds of fields that combine to a moderate-sized solid angle, although nothing approaching the entire sky. The disadvantages of this approach are that the solid angle is not contiguous and that there may remain some residual bias from the target selection since there is large-scale structure in the universe (i.e., the "serendipitous" objects may be associated with the target). The prototype for these serendipitous surveys was constructed in the 1980s from the *Einstein Observatory* data and is denoted the *Einstein* Extended Medium-Sensitivity Survey (EMSS; Gioia et al. 1990; Stocke et al. 1991). Recently, a number of EMSS-like surveys have been compiled from the *ROSAT* pointed data. The one most similar to the EMSS is the *ROSAT* International X-ray/Optical Survey (RIXOS; Mason et al. 2000). Other recent *ROSAT* surveys aimed at finding clusters of galaxies are cited in the caption to Figure 2 below.

These new surveys are about a factor of 2–4 deeper than the EMSS but still have the disadvantages mentioned above as well as containing some duplication of effort among them. In addition to the usual pointed program, *ROSAT* was the first X-ray–imaging experiment to survey the entire sky, compiling the X-ray equivalent of the Palomar Observatory Sky Survey (Trümper 1983; Voges et al. 1999; Schwope et al. 2000). These *ROSAT* All-Sky Survey (RASS) data have a substantial increase in sensitivity and source location accuracy over all previous X-ray all-sky surveys. RASS photons and other data products are available via the Internet.[3]

Earth-orbiting satellites must point their solar panels at the Sun. The Earth is in the ecliptic, so the natural scan pattern for satellites with fixed panels is circles of nearly constant ecliptic longitude that repeatedly pass over the ecliptic poles resulting in very deep exposures there. The South Atlantic Anomaly degrades the exposure at the south ecliptic pole, and the Large Magellanic Cloud obscures the extragalactic sky in this direction. The north ecliptic pole (NEP) is an undistinguished spot at moderate galactic latitude with moderate extinction. Its galactic coordinates are $l = 96\overset{\circ}{.}4$, $b = 29\overset{\circ}{.}8$; its supergalactic coordinates are $l_{SG} = 33\overset{\circ}{.}4$, $b_{SG} = 38\overset{\circ}{.}3$; and its neutral hydrogen column density is 4.3×10^{20} cm^{-2} (Elvis, Lockman, & Fassnacht 1994). The NEP is thus a good target for deep, unbiased, contiguous surveys, and many satellites, including *IRAS*, *COBE*, and *ROSAT*, have made them there.

We have constructed the *ROSAT* NEP Survey and have identified and obtained redshifts for more than 99% of the objects in it. The survey is as deep as the *ROSAT* serendipitous surveys and covers a comparable solid angle, but it is also contiguous. Some initial work on individual sources may be found in Henry

[1] Visiting Astronomer at the Canada-France-Hawaii Telescope, operated by the National Research Council of Canada, le Centre National de la Recherche Scientifique de France, and the University of Hawai'i, and at the W. M. Keck Observatory, jointly operated by the California Institute of Technology, the University of California, and the National Aeronautics and Space Administration.

[2] Istituto di Radioastronomia, CNR, via Gobetti 101, I-40129 Bologna, Italy.

[3] See http://wave.xray.mpe.mpg.de/rosat/survey.

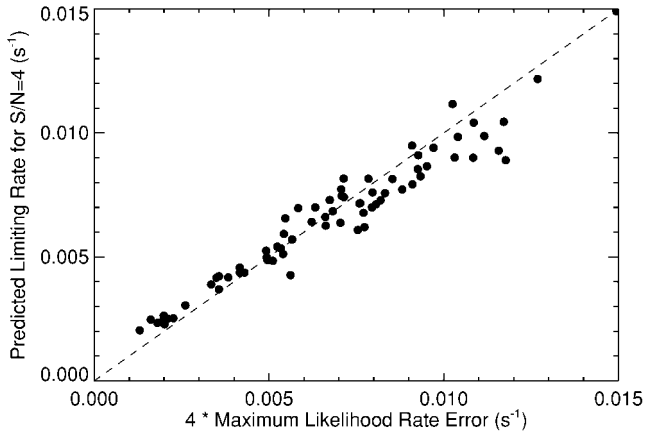

FIG. 1.—Data used to determine the effective detect cell radius for the NEP Survey. The maximum likelihood procedure determines the error on the detected count rate. The model given by eq. (1) predicts this error. The figure shows how good the prediction is for 71 sources in the NEP survey region with rates measured with a significance between 3.8 σ and 4.2 σ.

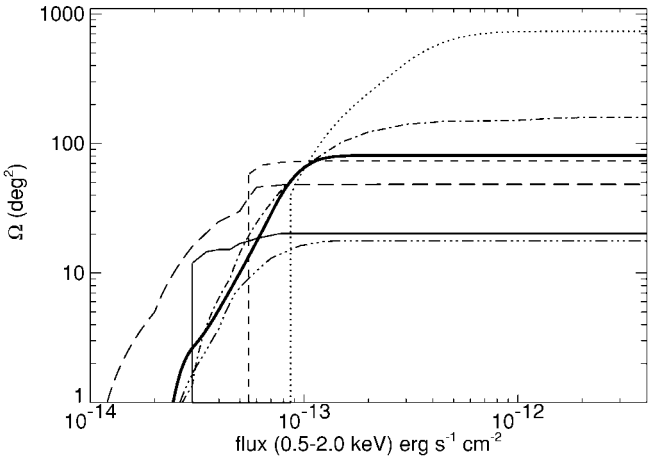

FIG. 2.—Sky coverage of various serendipitous surveys using pointed observations and of the NEP Survey using the RASS data reported here. The NEP sky coverage is denoted by the thick line and refers to fluxes that are accumulated in a 5′ radius region. References for the other surveys are, from top to bottom, Henry et al. (1992; the EMSS cluster survey, with the flux in the EMSS detect cell), Vikhlinin et al. (1998; the 160 deg^2 survey), H. Ebeling (2000, private communication; WARPS), Rosati et al. (2000; RDCS), Mason et al. (2000; RIXOS), and Burke et al. (1997; the SHARC Survey).

et al. (1994, 1995, 1997) and Gioia et al. (1995, 1999). In this Letter, we give an overview of the NEP results. Voges et al. (2001) give details of the X-ray data, Gioia et al. (2001) present evidence for cluster X-ray luminosity evolution in these data, and Mullis et al. (2001) describe how the NEP supercluster is delineated by these data. Future papers will provide the X-ray catalog, the optical identification catalog, and a catalog of X-ray–selected clusters in the NEP region.

2. SELECTION FUNCTION FOR THE *ROSAT* NEP SOURCES

One of the main objectives of the *ROSAT* mission was to conduct an all-sky X-ray survey with an imaging telescope. The satellite was launched on 1990 June 1, and the survey was mostly conducted from 1990 July 30 to 1991 January 25, with additional fill-in periods of a few days duration that covered most of the small fraction of the sky missed initially. The data used in our NEP work were extracted from the second processing (RASS-II) that featured improved attitude quality and fully merged photon data (see Voges et al. 1999 for details of this processing). We have chosen a contiguous region centered at the NEP bounded by $17^{\rm h}15^{\rm m} < \alpha(2000) < 18^{\rm h}45^{\rm m}$ and $62° < \delta(2000) < 71°$ totaling 80.7 deg^2. Over this region, the exposure variation was greater than a factor of 10, from less than 4000 to ~40,000 s, although the background variations in the same region and in our 0.1–2.4 keV band were small ($\pm 30\%$ variation peak to peak; Voges et al. 2001). Sources were detected using a multipass procedure involving sliding boxes of increasing sizes (with larger sizes used to find extended sources) to generate candidate source positions that were then input to a maximum likelihood fitter for final source selection and characterization. The maximum likelihood fitter weights each photon by the point-spread function at the energy and off-axis angle at which it was detected. Ultimately, 445 unique sources with net counts determined at greater than 4 σ comprise the NEP Survey. Voges et al. (2001) describe this selection procedure and the X-ray properties of these sources in more detail.

The survey selection function or sky coverage, i.e., the solid angle in which sources of a given flux could have been found, must be determined in order for the sample to be used for statistical studies. Background is an important effect at the NEP because of the more than factor of 10 increase in exposure there compared with the average of the RASS. The range of exposure variations is somewhat larger than that encountered in the remainder of the RASS as well. We have modeled the complicated detection process described in Voges et al. (1999) as a simple circular detect cell. The signal-to-noise ratio (S/N) on the source flux for this situation is

$$\frac{\rm S}{\rm N} = \frac{R_S T}{\sqrt{R_S T + R_B T \pi r_d^2}}, \qquad (1)$$

where R_S is the source counting rate, R_B is the background counting rate per square arcminute, T is the exposure time, and r_d is the detect cell radius in arcminutes. This relation assumes that the error on the determination of R_B is negligible as is true for the RASS since the background comes from a background map fitted to a 6.°4 × 6.°4 region (Voges et al. 2001).

We selected 71 sources from the NEP region that had R_S measured from the maximum likelihood fit with a significance between 3.8 σ and 4.2 σ. The detect cell radius was then chosen to provide the best agreement between the measured S/N and that predicted using equation (1) with the actual values of T and R_B at the positions of the 71 sources. We show this comparison in Figure 1 for our adopted detect radius of 1.′58. Our derived r_d corresponds to the ~60% encircled energy radius of the survey point-spread function (Boese 2000). Applying equation (1) with S/N = 4 and $r_d = 1.'58$ to the R_B and T maps of the NEP survey region (Voges et al. 2001) yields a map of the count rate R_S necessary to produce a 4 σ detection. We generated a 720 × 720 pixel map, converted R_S into flux as described by Voges et al. (2001), and then integrated over the map to obtain the selection function shown in Figure 2.

3. THE OPTICAL IDENTIFICATION PROGRAM

The X-ray data are the beginning; much more information is available after the sources are optically classified and their redshifts are determined. The NEP transits the meridian at mid-

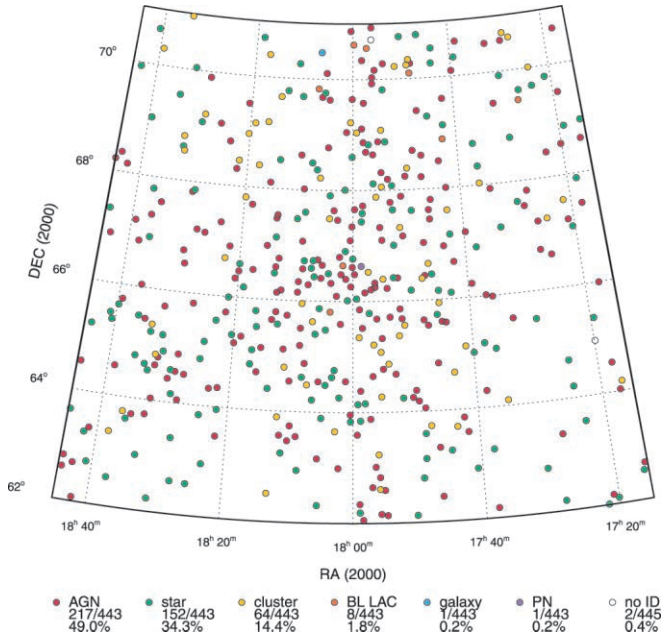

FIG. 3.—Identification content and distribution of sources in the NEP Survey

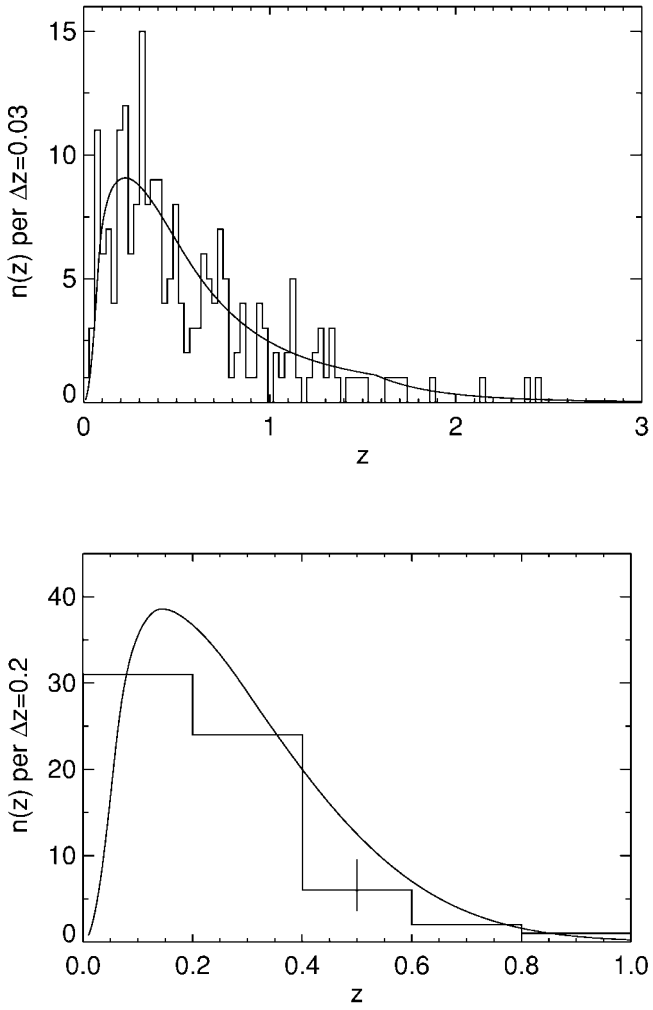

FIG. 4.—Redshift distribution of NEP sources compared with the distribution predicted by an evolving X-ray luminosity model. *Top*: AGNs with model from Miyaji et al. (2000). *Bottom*: Groups and clusters of galaxies with model from Rosati et al. (2000).

night in northern summer. The optical identification program began in the summer of 1991, a few months after the RASS was finished, and ended in the summer of 1999. We made most of the optical observations from Mauna Kea where 124 nights were assigned, of which 98 were clear. We spent 99 nights at the University of Hawai'i (UH) 2.2 m telescope, 17 nights at the Canada-France-Hawaii 3.6 m Telescope (CFHT), and eight nights at the Keck 10 m telescope. We made additional observations at Mount Hopkins where five nights at the Multiple Mirror Telescope were assigned, of which two were clear, and a clear night of 1.5 m time was also used.

The procedure used to identify an X-ray source is essentially that described in Stocke et al. (1991), although the process was considerably eased by the ~16 times smaller positional uncertainties of RASS compared with the *Einstein* IPC (16″ vs. ~60″). We began with finding charts prepared from the Automated Plate Measurement (APM) Facility object catalog (Hook et al. 1996). We also used data from the Digitized Sky Survey (DSS) to check the APM classifications. We obtained CCD imaging data with the UH 2.2 m telescope for fields that exhibited no objects in the X-ray error circle on the APM and DSS. We also imaged potential distant clusters (i.e., fields containing a few galaxies at the limits of the APM and DSS). Typical exposures were 10 minutes in B and I_C, although exposures of 30 minutes were sometimes obtained for sources that were eventually identified as distant clusters. M92 standards were used for the photometric calibration of the imaging data (Christian et al. 1985; Heasley & Christian 1986).

Next we obtained low-resolution spectra of objects near the X-ray position using the Wide Field Grism Spectrograph on the UH 2.2 m telescope, the Multi-Object Spectrograph on CFHT, and the Low Resolution Imaging Spectrograph on Keck II. We paid particular attention at the UH 2.2 m telescope to objects with APM colors $O-E \leq 1.2$ that were within 15″ of the X-ray source since they were almost always active galactic nuclei (AGNs). Using the number counts from Boyle, Shanks, & Peterson (1988), ~1.5 AGNs brighter than $B = 21.5$ are expected to lie by chance within the area formed by 15″ radius circles around all 445 objects in our sample, which is negligible. The strong AGN emission lines yielded a classifiable spectrum from short exposures with the UH 2.2 m telescope. We also used the UH 2.2 m telescope to obtain redshifts from long-slit spectra of relatively bright cluster galaxies. Finally, we obtained CFHT and Keck multiobject and Keck long-slit spectra of the X-ray sources that were near faint collections of galaxies. The multiobject spectroscopy was a departure from the Stocke et al. (1991) procedure. It provided more confidence in the cluster identifications since many concordant redshifts could be obtained. Spectrophotometric calibration came from standards from Oke & Gunn (1983) and Massey et al. (1988).

Figure 3 gives a summary of the identification program. Nearly half (49.0%) of all sources are AGNs. The next most common identifications are stars at 34.3%, while clusters and groups comprise 14.4% of the NEP sources. BL Lacertae objects are 1.8% of the sample. Only two sources are not identified, implying an identification rate of 99.6%. There is evidence that at least one of the two unidentified objects is a blend and that both may be statistical fluctuations given the selection criteria. One planetary nebula, NGC 6543, was detected as an X-ray source (Kreysing et al. 1992).

The content of the NEP Survey is remarkably similar to that

of the EMSS, which had 51% AGNs, 26% stars, 13% clusters (including "cooling flow galaxies"), and 5% BL Lac objects (Stocke et al. 1991; Rector et al. 2000). RIXOS (Mason et al. 2000) had a significantly higher fraction of AGNs (62%), significantly fewer stars (23%), and marginally significantly fewer clusters (9%, different at the 2.5 σ level) than the NEP Survey. The disagreement among the stellar fractions probably results from the NEP lying at a lower galactic latitude than the average EMSS or RIXOS field. The low RIXOS cluster content had been noted previously. Mason et al. (2000) estimate that it is a factor of ~2 low, which, when compensated, brings the RIXOS cluster fraction up to 16.4%, in good agreement with the NEP fraction of 14.4%.

Figure 4 gives the redshift distributions of AGNs and groups and clusters of galaxies in the NEP Survey. The median and highest redshift AGNs are 0.408 and 3.889, respectively. The median and most distant clusters are at $z = 0.205$ and 0.811, respectively. In the top panel of Figure 4, we compare the observed redshift distribution of NEP AGNs with that predicted from the evolving AGN X-ray luminosity function (XLF) of Miyaji, Hasinger, & Schmidt (2000). The agreement is quite good. The predicted versus observed numbers of AGNs in the redshift intervals 0.0–0.5, 0.5–1.0, and 1.0–3.0 are 119 versus 125, 69 versus 57, and 44 versus 34, respectively. A detailed description of the NEP AGN sample and the constraints it provides on the evolution of the X-ray XLF will be published in a future paper. In the bottom panel of Figure 4, we compare the observed NEP cluster and group redshift distribution with that predicted from the evolving cluster XLF of Rosati et al. (2000). The predicted versus observed numbers of clusters and groups in the redshift intervals 0.0–0.3 and 0.3–0.85 are 45.8 versus 45 and 28.4 versus 19, respectively. The observations in the higher redshift shell disagree with the best-fit model of Rosati et al. (2000) at ~2 σ, and they disagree with a no-evolution model at ~6 σ. Including the errors on the Rosati et al. evolution model parameters brings it into agreement with the NEP observations. An initial discussion of evolution in the NEP cluster sample is in Gioia et al. (2001), and the details will be presented in future papers.

4. THE NEP log $N(>S)$–log S DISTRIBUTIONS

The traditional first look at the results of a survey includes the integral number counts or log $N(>S)$–log S distribution. For X-ray surveys, which have a mix of source types as well as extended objects, the distribution for all sources together is not very illuminating. An optical identification program permits the classification of sources as well as provides the redshift to the extended cluster sources so that their total flux can be determined from that provided by the detection algorithm.

In Figure 5, we show the NEP Survey log $N(>S)$–log S distribution for AGNs (excluding BL Lac objects), clusters and groups of galaxies, and BL Lac objects alone. We constructed the NEP distributions from

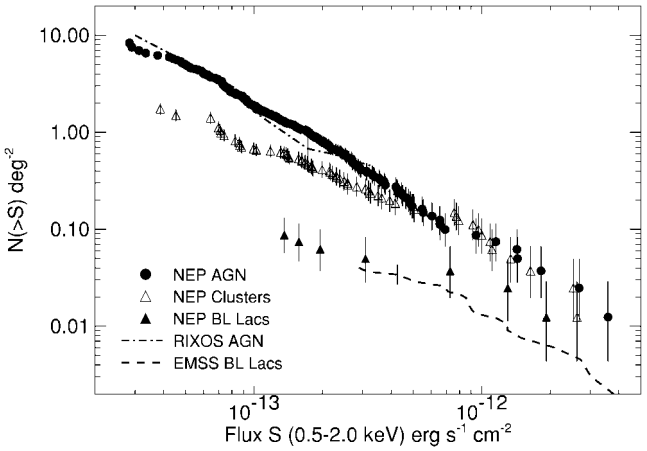

FIG. 5.—The log $N(>S)$–log S distributions for NEP AGNs (excluding BL Lac objects), groups and clusters of galaxies, and BL Lac objects compared with previously measured distributions for AGNs and BL Lac objects.

$$N(>S) = \sum_{S_i > S} \frac{1}{\Omega(S_i)}, \qquad (2)$$

where $\Omega(S_i)$ is the sky coverage at flux S_i from Figure 2. Also shown in Figure 5 are the AGN distribution from RIXOS (Mason et al. 2000) and the EMSS BL Lac distribution from the M91 sample of Rector et al. (2000). The D40 sample of Rector et al. is larger, but no sky coverage was provided for it. The previous measurements agree with our results. This agreement and the one presented in Gioia et al. (2001) of the NEP cluster distribution with other cluster determinations lend support to the accuracy of our sky coverage. The different slopes of the AGNs, clusters and groups of galaxies, and BL Lac distributions illustrate the different evolutionary properties of these objects.

We thank the University of Hawai'i TAC for its generous support of this program for nearly a decade. The staffs of the University of Hawai'i, Canada-France-Hawaii, and Keck telescopes performed with their customary professionalism. Many thanks are also due to the *ROSAT* team, particularly Günther Hasinger and Joachim Trümper. We are grateful to our sponsors who have enabled this project. Support has come from the Bundesministerium für Bildung und Forschung (BMBF/DLR), the Max-Planck-Gesellschaft (MPG), the NSF (AST 91-19216 and AST 95-00515), NASA (NGT5-50175, GO-5402.01-93A, and GO-05987.02-94A), the Smithsonian Institution, NATO (CRG91-0415), and the Italian ASI-CNR.

REFERENCES

Boese, F. G. 2000, A&AS, 141, 507
Boyle, B. J., Shanks, T., & Peterson, B. A. 1988, MNRAS, 235, 935
Burke, D. J., Collins, C. A., Sharples, R. M., Romer, A. K., Holden, B. P., & Nichol, R. C. 1997, ApJ, 488, L83
Christian, C. A., Adams, M., Barnes, J. V., Butcher, H., Hayes, D. S., Mould, J. R., & Siegel, M. 1985, PASP, 97, 363
Cooke, B. A., et al. 1978, MNRAS, 182, 489
Elvis, M., Lockman, F. J., & Fassnacht, C. 1994, ApJS, 95, 413
Forman, W., Jones, C., Cominsky, L., Julien, P., Murray, S., Peters, G., Tananbaum, H., & Giacconi, R. 1978, ApJS, 38, 357
Gioia, I. M., et al. 1995, A&A, 297, L75
Gioia, I. M., Henry, J. P., Mullis, C. R., Ebeling, H., & Wolter, A. 1999, AJ, 117, 2608
Gioia, I. M., Henry, J. P., Mullis, C. R., Voges, W., Briel, U. G., Böhringer, H., & Huchra, J. P. 2001, ApJ, 553, L105
Gioia, I. M. Maccacaro, T., Morris, S. L., Schild, R. E., Stocke, J. T., Wolter, A., & Henry, J. P. 1990, ApJS, 72, 567
Heasley, J. N., & Christian, C. A. 1986, ApJ, 307, 738
Henry, J. P., et al. 1994, AJ, 107, 1270
———. 1995, ApJ, 449, 422

Henry, J. P., Gioia, I. M., Maccacaro, T., Morris, S. L., Stocke, J. T., & Wolter, A. 1992, ApJ, 386, 408
Henry, J. P., et al. 1997, AJ, 114, 1293
Hook, I. M., McMahon, R. G., Irwin, M. J., & Hazard, C. 1996, MNRAS, 282, 1274
Kreysing, H. C., Diesch, C., Zweigle, J., Staubert, R., Grewing, M., & Hasinger, G. 1992, A&A, 264, 623
Mason, K. O., et al. 2000, MNRAS, 311, 456
Massey, P., Strobel, K., Barnes, J. V., & Anderson, E. 1988, ApJ, 328, 315
Miyaji, T., Hasinger, G., & Schmidt, M. 2000, A&A, 353, 25
Mullis, C. R., Henry, J. P., Gioia, I. M., Böhringer, H., Briel, U. G., Voges, W., & Huchra, J. P. 2001, ApJ, 553, L115
Oke, J. B., & Gunn, J. E. 1983, ApJ, 266, 713
Piccinotti, G., Mushotzky, R. F., Boldt, E. A., Holt, S. S., Marshall, F. E., Serlemitsos, P. J., & Shafer, R. A. 1982, ApJ, 253, 485
Rector, T. A., Stocke, J. T., Perlman, E. S., Morris, S. L., & Gioia, I. M. 2000, AJ, 120, 1626
Rosati, P., Borgani, S., Della Ceca, R., Stanford, A., Eisenhardt, P., & Lidman, C. 2000, in Large-Scale Structure in the X-Ray Universe, ed. M. Plionis & I. Georgantopoulos (Paris: Atlantisciences), 13
Schwope, A. D., et al. 2000, Astron. Nachr., 321, 1
Stocke, J. T., Morris, S. L., Gioia, I. M., Maccacaro, T., Schild, R. E., Wolter, A., Fleming, T. A., & Henry, J. P. 1991, ApJS, 76, 813
Trümper, J. 1983, Adv. Space Res., 27, 1404
Vikhlinin, A., McNamara, B. R., Forman, W., Jones, C., Quintana, H., & Hornstrup, A. 1998, ApJ, 502, 558
Voges, W., et al. 1999, A&A, 349, 389
Voges, W., Henry, J. P., Briel, U. G., Böhringer, H., Mullis, C. R., Gioia, I. M., & Huchra, J. P. 2001, ApJ, 553, L119
Wood, K. S., et al. 1984, ApJS, 56, 507